

Thermoelectric Signatures of Time-Reversal Symmetry Breaking States in Multiband Superconductors

Julien Garaud,¹ Mihail Silaev,¹ and Egor Babaev¹

¹*Department of Theoretical Physics and Center for Quantum Materials,
KTH-Royal Institute of Technology, Stockholm, SE-10691 Sweden**

(Dated: March 18, 2016)

We show that superconductors with broken time-reversal symmetry have very specific magnetic and electric responses to inhomogeneous heating. A local heating of such superconductors induces a magnetic field with a profile that is sensitive to the presence of domain walls and crystalline anisotropy of superconducting states. A nonstationary heating process produces an electric field and a charge imbalance in different bands. These effects can be measured and used to distinguish $s + is$ and $s + id$ superconducting states in the candidate materials such as $\text{Ba}_{1-x}\text{K}_x\text{Fe}_2\text{As}_2$.

PACS numbers: 74.25.fg, 74.20.Rp

In many recently discovered superconducting materials, the pairing of electrons is supposed to take place in several sheets of a Fermi surface formed by overlapping electronic bands [1–6]. Of special interest are the states where the difference of gap's phases in the bands is neither 0 or π [7–18]. Indeed, in addition to the breakdown of usual $U(1)$ gauge symmetry, such superconducting states are characterized by an extra broken time-reversal symmetry (BTRS) that has numerous interesting physical consequences, many of which are not yet explored. Iron-based superconductors [3] are among the most commonly accepted candidates for the observation of a BTRS state originating from the multiband character of superconductivity and several competing pairing channels.

Experimental data suggest that in the hole-doped 122 compounds $\text{Ba}_{1-x}\text{K}_x\text{Fe}_2\text{As}_2$ the symmetry of the superconducting state can change depending on the doping level x . At moderate doping $x \sim 0.4$ various measurements including neutron scattering [19], thermal conductivity [20], and angle-resolved photoemission spectroscopy (ARPES) [21–23] are consistent with the hypothesis of the s_{\pm} state where the superconducting gap changes sign between electron and hole pockets. On the other hand, the symmetry of the superconducting state at heavy doping $x \rightarrow 1$ is not so clear regarding the question of whether the d channel dominates or if the gap retains s_{\pm} symmetry changing sign between the inner hole bands at the Γ point [24, 25]. Indeed, there are evidences that d -wave pairing channel dominates [26–29], while other ARPES data were interpreted in favor of an s -wave symmetry [30, 31].

Which of these two possibilities is realized at heavy doping depends on the fine balance of the pairing interactions in different channels. However, both cases strongly suggest the existence of an intermediate superconducting state that breaks time-reversal symmetry at a certain range of the doping level x . Two alternative scenarios

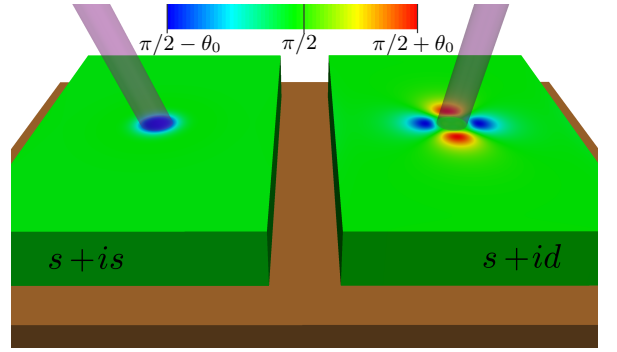


Figure 1: Variation of the interband phase difference θ_{12} in BTRS three-band superconductors induced by a hot spot created, e.g., by a laser pulse. The phase difference variation induced by temperature gradients around hot spots in the case of an $s + is$ state (left) preserves C_4 symmetry, while it has fourfold structure for an $s + id$ state. The value of θ_0 in the $s + is$ case is 0.18 while for $s + id$ it is smaller: $\theta_0 = 0.05$.

have been considered: namely, $s + id$ and $s + is$ symmetries [8, 9, 17, 30, 31]. The $s + id$ state is anisotropic, as it breaks C_4 crystalline symmetry, while the $s + is$ state is qualitatively different as C_4 symmetry is preserved [17]. Note that the $s + id$ state is qualitatively different from the (time-reversal-preserving) $s + d$ state which earlier attracted interest in the context of high-temperature cuprate superconductors (see, e.g., [32–35]). It also contrasts with the $d + id$ state that violates both parity and time-reversal symmetries [7, 36].

To this day, no experimental proof of $s + is$ or $s + id$ BTRS states has been reported. Indeed, probing the relative phases between components of the order parameter in different bands is a challenging task. For example, the $s + is$ state does not break point group symmetries and therefore it is not associated with intrinsic Cooper pair angular momentum. Hence, it cannot produce a local magnetic field and is invisible for conventional methods like muon spin relaxation and polar Kerr effect measurements that were used to search for BTRS $p + ip$ superconducting state in, e.g., the Sr_2RuO_4 compound

*Electronic address: garaud.phys@gmail.com

[37]. Proposals for indirect observation of a BTRS signature in pnictides, with various limitations, have been recently voiced. These include, for example, investigation of the spectrum of collective modes which includes massless [14] and mixed phase-density [15, 17, 38, 39] excitations. It was also proposed to consider exotic topological excitations in the form of skyrmions and domain walls [40–42], an unconventional vortex viscosity mechanism [43], vortex clustering [15], and exotic reentrant and precursor phases induced by fluctuations [44–47]. Spontaneous currents were predicted to exist near impurities in anisotropic superconducting states [8, 18] or in samples subjected to strain [18]. The latter proposal actually involves symmetry change of $s+is$ states and relies on the presence of disorder, which usually has an uncontrollable distribution.

In this Letter, we discuss an experimental set-up based on a local heating, that allows the direct observation of BTRS states in a controllable way. This is illustrated in Fig. 1, where local heating induces a local variation of relative phases that are further shown to yield electromagnetic excitations. The key idea is based on the recent proposal of an unconventional thermoelectric effect in BTRS multiband superconductors [48]. There, a temperature gradient generates phase gradients of condensate components, due to the generically temperature-dependent interband phase differences $\theta_{ki}(T) := \theta_k - \theta_i$ (where k, i are band indices). It results that the local heating generates spontaneous magnetic fields and charge imbalance distributions. These thermoelectric responses are drastically different from their counterparts in conventional superconductors [49]. As discussed below, the fields created by local heating have opposite directions in two degenerate superconducting states [i.e. $s + is(d)$ and $s - is(d)$ ones]. They are measurable by conventional techniques (e.g. by SQUID) and therefore scans of the surface can be used to diagnose the structure of order parameter and interband phase differences, to detect pinned domain walls or broken crystalline symmetry states in either $s + is$ or $s + id$ superconductors.

We consider a minimal three-band microscopic model which has been suggested to describe the BTRS superconducting state in the hole-doped 122 iron-pnictide compounds [10, 17, 39] with three distinct superconducting gaps $\Delta_{1,2,3}$ in different bands. The pairing which leads to the BTRS state is dominated by the competition of different interband repulsion channels described by the following coupling matrix:

$$\hat{g} = -\nu_0 \begin{pmatrix} 0 & \eta & \lambda \\ \eta & 0 & \lambda \\ \lambda & \lambda & 0 \end{pmatrix}. \quad (1)$$

Here, we assume for simplicity that the density of states ν_0 is the same in all superconducting bands. This model has been suggested [10, 17, 39] in order to describe transitions between s/s_{\pm} and $s+is$ states when tuning parameters η, λ and temperature. The dimensionless coefficients η and λ describe different pairing channels, whether it

is an $s + is$ or an $s + id$ state. In the former case $\Delta_{1,2}$ correspond to the gaps at hole Fermi surfaces and Δ_3 is the gap at the electron pockets, so that $u_{hh} = \nu_0\eta$ and $u_{eh} = \nu_0\lambda$ are, respectively, the hole-hole and electron-hole interactions [17, 39]. The same model (1) can be used to describe the $s + id$ states but there, $\Delta_{1,2}$ describe gaps in electron pockets and Δ_3 is the gap at the hole Fermi surface, so that $u_{eh} = \nu_0\lambda$ and $u_{ee} = \nu_0\eta$ are electron-hole and electron-electron interactions respectively.

To study magnetic and electric responses of both $s + is$ and $s + id$ states, we use a Time-Dependent Ginzburg-Landau (TDGL) approach [50, 51] generalized to a multiband case (see derivation in Appendix A and B). The dimensionless TDGL equations read (see details in [67]):

$$(\partial_t + 2i\tilde{e}\varphi)\psi_k = -\frac{\delta\mathcal{F}}{\delta\psi_k^*}, \quad \nabla \times \mathbf{B} - \sigma_n \mathbf{E} = \mathbf{j}_s, \quad (2)$$

where φ is the electrostatic potential, σ_n is the normal state conductivity, and $\mathbf{j}_s = -\delta\mathcal{F}/\delta\mathbf{A}$ is the superconducting current. Near the critical temperature the energy relaxation is determined by the phonon scattering which yields the relaxation time scale $t_0 = \pi\hbar/(8T_c) \sim 1$ ps provided $T_c \sim 1$ meV, which is about 10 K.

Note that multiband superconductors are described by several components ψ_k which do not necessarily coincide with the gap functions Δ_i in different bands (see, e.g., [17, 39]). For example, since the coupling matrix (1) has only two positive eigenvalues, the relevant Ginzburg-Landau (GL) theory reduces to a two-component one (see details in Appendix A), which in dimensionless units reads as

$$\mathcal{F} = \frac{B^2}{8\pi} + \sum_{j=1}^2 \left(k_j |\Pi\psi_j|^2 + \alpha_j |\psi_j|^2 + \frac{\beta_j}{2} |\psi_j|^4 \right) \quad (3a)$$

$$+ k_{12,a} (\Pi_a^* \psi_1^* \Pi_a \psi_2 + c.c.) \quad (3b)$$

$$+ \gamma |\psi_1|^2 |\psi_2|^2 + \frac{\delta}{2} (\psi_1^{*2} \psi_2^2 + c.c.), \quad (3c)$$

with $\Pi = \nabla - 2i\tilde{e}\mathbf{A}$. The components $\psi_{1,2}$ are determined by a superposition of the different gap functions Δ_i . All coefficients of the model (3) are consistently determined from the microscopic coupling matrix (see details in Appendix A), and the temperature dependence is given by the coefficients:

$$\alpha_1 = -2(G_0 - G_1 + \tau) \quad (4a)$$

$$\alpha_2 = -(2x^2 + 1)(G_0 - G_2 + \tau) \quad (4b)$$

where $\tau = (1 - T/T_c)$, $x = (\eta - \sqrt{\eta^2 + 8\lambda^2})/(4\lambda)$, $G_{1,2}$ are the positive eigenvalues of the inverse coupling matrix $\nu_0\hat{g}^{-1}$ and $G_0 = \min(G_1, G_2)$. The general GL functional (3) derived from the three-band microscopic model has $\delta > 0$. Hence it favors BTRS with $\pm\pi/2$ phase differences between ψ_1 and ψ_2 order parameter components, which describes both the $s + is$ and $s + id$ states depending on the structure of mixed gradient terms (3b). They are

$k_{12,x} = k_{12,y}$ for the $s + is$ state and $k_{12,x} = -k_{12,y}$ for the crystalline C_4 -symmetry breaking $s + id$ state.

As a consequence of the discrete degeneracy due to BTRS, the model (3c) allows domain walls (DW) interpolating between regions with different relative phases. The direct observation of DWs in $s + is(d)$ states is challenging. Unlike DWs in $p + ip$ superconductors, they do not generate a spontaneous magnetic field. However, by our general argument below, DWs should provide a controlled magnetic response in the presence of relative-density perturbations that can be induced by a local heating.

To investigate the response to spatial modulations of the components of the order parameter induced by a local heat source, the fields $\psi_{1,2}$ and \mathbf{A} are discretized using a finite-element framework [54] (see discussion of numerical methods in Appendix C). To model the local heating, the temperature profile is found by solving the (stationary) heat equation for a heat source at temperature T_s , while boundaries are kept at $T_0 = 0.7T_c$. Once the temperature profile is found, the coefficient α_k in (3) varies in space and the TDGL equations (2) are evolved for $\Delta t = 80$ (in units t_0 defined above). The temperature of the heat source is then modified to T'_s , and the TDGL equations are further evolved for the new temperature profile for a period Δt . The temperature of the source is initially set to T_0 , sequentially ramped up to $0.95T_c$, and then ramped down back to T_0 . In our simulations, we chose the dimensionless conductivity $\sigma_n = 0.1$ and the coupling constant $\tilde{e} = 0.113$. The coefficients in GL functional (3) are determined using the microscopic coupling matrix (1) with coefficients $\eta = 5$ and $\lambda = 4.5$ [68].

As shown in Fig. 2, according to the simulations, when the source heats up a domain wall, it induces a multipolar magnetic field with zero net flux. In the case of a superconductor with $s + is$ symmetry, it shows a dipolar structure, while it is differently distributed for $s + id$. On the other hand, when the heat source is focused on the uniform $s + is$ state it shows no magnetic response, while a fourfold magnetic field is induced in the $s + id$ case as a result of the explicit breakdown of the C_4 symmetry. Here, spatial variations are normalized to the penetration depth λ_L and the amplitudes of the induced magnetic field to the second critical field H_{c2} defined by the GL functional (3). Provided the typical values of $H_{c2} \sim 10\text{T}$ in 122 pnictides [56], one can see that the magnetic response can be detected with high accuracy by conventional local probes of static magnetic field such as scanning SQUID or Hall probe microscopy.

The physical origin of the spontaneous magnetic response follows from that the total current is the sum of partial currents in each of the N bands $\mathbf{j} = \sum_{k=1}^N \mathbf{j}_k$ and therefore can be generated by the gradients of relative phases [48]. Since $\mathbf{j}_k = (\nabla\theta_k - 2\pi\mathbf{A}/\Phi_0)c\Phi_0/(8\pi^2\lambda_k^2)$ the London expression for the magnetic field in multi-

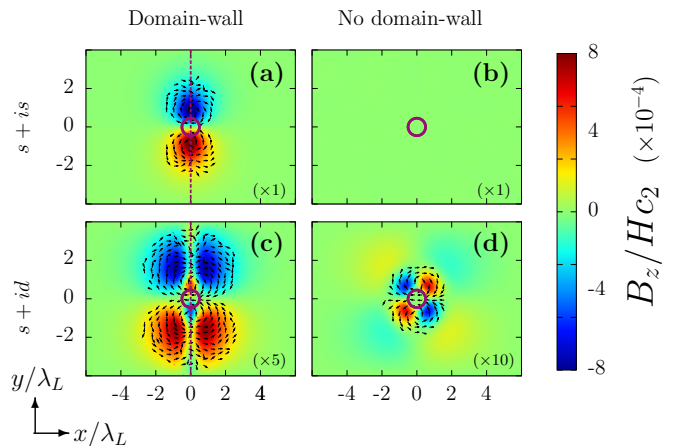


Figure 2: The magnetic response that originates in local heating of the sample. Panels (a) and (c), respectively, show the response when a local hot spot heats an area of a sample which contains a domain wall. Here, we display two cases of the domain walls for two BTRS states: $s + is$ and $s + id$. Panels (b) and (d) show the response to the local hot spot in the case of the homogeneous BTRS state for the $s + is$ and $s + id$ superconducting state. The color plot shows the magnitude of the out-of-plane induced magnetic field B_z (magnitudes differ in different panels), while arrows indicate the orientation of supercurrents. The dotted line indicates the presence of the domain wall and the inhomogeneous temperature profile is induced by the ringlike heat source shown by the small circles. Length scales are given in terms of London penetration length and calculated values of the GL parameters are given in [52, 55] and Appendix A-C.

band superconductors is modified as follows

$$\mathbf{B} = -\frac{4\pi}{c}\nabla \times (\lambda_L^2 \mathbf{j}) + \frac{\Phi_0}{2\pi N} \sum_{k>i} \nabla \times (\gamma_{ki} \nabla \theta_{ki}) \quad (5)$$

where λ_k are coefficients characterizing contribution of each band to the Meissner screening, $\lambda_L = 1/\sqrt{\sum_k \lambda_k^{-2}}$ is the London penetration depth and $\gamma_{ki}(\mathbf{r}) = \lambda_L^2 (\lambda_k^{-2}(\mathbf{r}) - \lambda_i^{-2}(\mathbf{r}))$. In contrast to London's magnetostatics, Eq. (5) shows that the magnetic field features an additional contribution when relative density gradients $\nabla \gamma_{ki}(\mathbf{r})$ are noncollinear with that of relative-phase gradients $\nabla \theta_{ki}$. Such gradients generically appear in BTRS states if a domain wall-containing superconductor is exposed to a local heat source. The second term in (5) can be nonzero even in the absence of domain walls due to direction dependent tensor coefficients $\hat{\gamma}_{ki}(\mathbf{r})$ in anisotropic $s + id$ states.

Domain walls can be created by quenching the sample and stabilized by pinning or artificial geometric barriers [42, 57]. Yet it is also important to obtain the evidence of isotropic $s + is$ states for homogeneous superconducting states. Below, we show that this can be done by considering the nonequilibrium electric responses generated by nonstationary heating when the local temperature evolves recovering from the initial hot spot created,

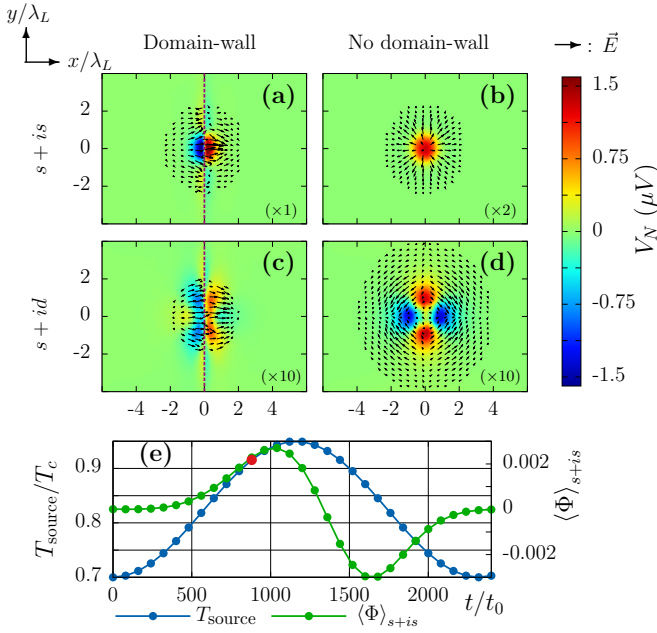


Figure 3: Electric response due to the nonstationary heating of the sample. Panel (e) shows the time evolution of the source’s temperature. Panels (a)-(d) correspond to the cases in Fig. 2 and the color plot shows the voltage V_N generated by the charge imbalance that can be picked by a normal detector, while the arrows correspond to the electric field. Panel (e) also displays Φ integrated over the whole sample, of an $s + is$ superconductor without DW (b). The red dot on panel (e) denotes the “position” of panels (a)-(d) in the time series.

e.g., by a laser pulse [49]. An unusual electric response can be seen when combining Eq.(5) to Faraday’s law. The electric field $\mathbf{E} = -c^{-1}\partial_t \mathbf{A} - \nabla \varphi$ can be rewritten as

$$\mathbf{E} = \frac{4\pi}{c^2} \frac{\partial}{\partial t} (\lambda_L^2 \mathbf{j}) - \frac{\Phi_0}{2\pi N c} \sum_{k>i} \frac{\partial}{\partial t} (\gamma_{ki} \nabla \theta_{ki}) - \nabla \Phi. \quad (6)$$

Here, $\Phi = \sum_k (\varphi + \hbar \dot{\theta}_k / 2e) / N$ is a gauge invariant potential field, determined by the sum of chemical potential differences between quasiparticles $\mu_q = e\varphi$ and condensates in each band $\mu_p^{(k)} = -\hbar \dot{\theta}_k / 2$. Each of the partial potential differences $\Phi^{(k)} = [\mu_q - \mu_p^{(k)}] / e$ is proportional to charge imbalance in the k -th band $Q_k^* = 2e^2 \nu_0 \Phi^{(k)}$ [58–60]. In multicomponent systems the charge imbalance can be generated by variations of interband phase differences in space and time. The physics behind this process is a nonequilibrium redistribution of Cooper pairs between different bands which initially creates partial charge imbalances Q_k^* . This mechanism leads to the unconventional electric response of BTRS superconductors to a nonstationary local heating. It can be measured with potential probe techniques that were employed to study the imbalance between quasiparticles and condensate subsystems in conventional superconductors [61, 62].

Fig. 3 shows such an electric response to a nonstationary heating of the superconducting sample. This multi-

component electrodynamic phenomenon can be used to detect BTRS states through charge imbalance generation in response to nonstationary heating. As shown in Fig. 3, the charge imbalance shows nontrivial pattern that is different for $s + is$ and $s + id$ states. The total charge imbalance $\langle \Phi \rangle$ in uniform $s + id$ is zero as a result of the fourfold symmetric structure due to broken C_4 symmetry. On the other hand, as shown in Fig. 3(e), $\langle \Phi \rangle \neq 0$ in uniform $s + is$. Note that the total imbalance in the case of domain walls Fig. 3(a) and Fig. 3(c) is zero because the heat source is centered at the domain wall. A shifted source from the DW center will not be symmetric and thus its average will not vanish.

The generated charge imbalance can be measured with the standard technique using the normal metal and superconducting potential probes [61, 62]. The magnitude of voltage V_N induced in the normal detector is related to the dimensionless signal shown in Fig. 3 as $V_N = \hbar \Phi / (t_0 e)$, where $\hbar / (t_0 e) \approx 4 \text{ mV}$. The overall magnitude of the voltage signal is thus expected at the order of the μV . The electric field and charge imbalance depend on the dynamics of the temperature profile variation, while \mathbf{B} depends on the temperature profile itself. As a result, the sign of the induced electric field and charge imbalance changes when ramping down the heat-source temperature, while it does not for the magnetic field (see animations [63] and their description in Appendix D). Note that similarly to the spontaneous magnetic field, the induced charge imbalances are sensitive to BTRS: degenerate $s + is$ and $s - is$ states produce opposite electric fields and charge imbalances in response to the same heating protocol. It allows to discriminate between the usual thermoelectric occurring in conventional superconductors and the unconventional one being a specific signature of BTRS states.

To conclude, we demonstrated possible direct manifestations of BTRS states in experimentally observable electric and magnetic responses to nonuniform and nonstationary heating. The signs of the generically induced magnetic field and charge imbalance distributions are opposite in degenerate BTRS states [i.e. in $s + is(d)$ and $s - is(d)$]. These specific thermoelectric behaviors were also shown to reveal the presence of domain walls between $s + is(d)/s - is(d)$ states. Moreover, the demonstrated crucial dependence of thermomagnetic and charge imbalance responses on crystalline anisotropy provides an experimental tool to distinguish between isotropic $s + is$ and C_4 symmetry-breaking $s + id$ states that are particularly interesting for pnictides.

Acknowledgments

The work was supported by the Swedish Research Council Grants No. 642-2013-7837. The computations were performed on resources provided by the Swedish National Infrastructure for Computing (SNIC) at the National Supercomputer Center at Linköping, Sweden.

Appendix A: Ginzburg-Landau expansion for the $s + is$ and $s + id$ superconductors

We consider here two alternative patterns of superconducting coupling which both result on BTRS state but will be shown to yield qualitatively different physical properties. In the first scheme shown in Fig. 4(a) the dominating pairing channels are the interband repulsion between electron and hole bands, as well as between two hole pockets at Γ . There, the order parameter is the same in both electron pockets so that the crystalline C_4 symmetry is not broken and thus corresponds to an s state. Instead the second alternative shown in Fig. 4(b) is that when the strongest interactions are the repulsions between hole and electron bands and between two electron pockets. Such interaction favours order parameter sign change between electron pockets resulting in a C_4 symmetry breaking d -wave state.

To derive the Ginzburg-Landau expansion that is used in our simulations, we consider the microscopic model of clean superconductor with three overlapping bands at the Fermi level. Within quasiclassical approximation the band parameters characterizing the two different cylindrical sheets of the Fermi surface are the Fermi velocities $v_F^{(j)}$ and the partial densities of states (DOS) ν_j , labelled by the band indices $j = 1, 2, 3$. To describe the two possible alternatives of BTRS states, namely $s + is$ and $s + id$ symmetries, we consider two three-band models schematically shown in Fig. 4. The Eilenberger equations for quasiclassical propagators take the form

$$\hbar \mathbf{v}_F^{(j)} \mathbf{\Pi} f_j + 2\omega_n f_j - 2\Delta_j g_j = 0, \quad (\text{A.1})$$

$$\hbar \mathbf{v}_F^{(j)} \mathbf{\Pi}^* f_j^+ - 2\omega_n f_j^+ + 2\Delta_j^* g_j = 0,$$

where $\mathbf{\Pi} = \nabla - 2\pi i \mathbf{A}/\Phi_0$, \mathbf{A} is the vector potential, $\mathbf{v}_F^{(j)}$ is the Fermi velocity. The quasiclassical Green's functions in each band obey normalization condition $g_j^2 + f_j f_j^+ = 1$. The self-consistency equations for the gaps and electric current are

$$\Delta_i(\mathbf{p}, \mathbf{r}) = 2\pi T \sum_{n, \mathbf{p}', j} \lambda_{ij}(\mathbf{p}, \mathbf{p}') f_j(\mathbf{p}, \mathbf{r}, \omega_n) \quad (\text{A.2})$$

$$\mathbf{j}(\mathbf{r}) = 2\pi e T \nu \sum_{n, \mathbf{p}, j} \mathbf{v}_F^{(j)} \text{Im } g_j(\mathbf{p}, \mathbf{r}, \omega_n) \quad (\text{A.3})$$

where $g_j = \text{sign}(\omega_n) \sqrt{1 - f_j f_j^+}$ and ν is the density of states, \mathbf{p} parameters run over the corresponding Fermi surfaces and λ_{ij} is the coupling potential matrix. For simplicity we will consider further isotropic pairing states so that $\lambda_{ij}(\mathbf{p}, \mathbf{p}') = \text{const}$ on each of the Fermi surfaces. However in electron pockets we keep the anisotropy of Fermi velocities in Eq.(A.1). We neglect the anisotropy of hole bands which is a well-justified assumption [64].

The derivation of the GL functional from the microscopic equations formally follows the standard scheme. First we find the solutions of Eqs.(A.1) in the form of

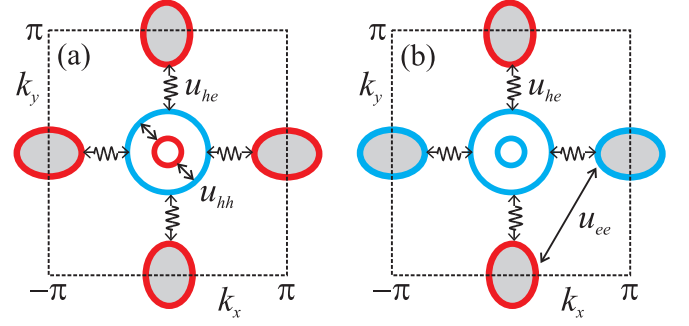


Figure 4: (Color online) – Schematic view of the band structure in hole-doped iron pnictide compound $\text{Ba}_{1-x}\text{K}_x\text{Fe}_2\text{As}_2$. It consists of two hole pockets at Γ shown by open circles and two electron pockets at $(0; \pi)$ and $(\pi; 0)$ shown by filled ellipses. In panel (a), the $s + is$ state is favored by superconducting coupling dominated by the interband repulsion between electron and hole Fermi surfaces u_{he} , as well as between the two hole pockets u_{hh} . In panel (b), there is a possibility of $s + id$ state due to the repulsion between electron and hole Fermi surfaces u_{he} as well as between electron pockets u_{ee} .

the expansion by powers of the gap functions amplitudes Δ_j and their gradients:

$$f_j(\mathbf{p}, \mathbf{r}, \omega_n) = \quad (\text{A.4})$$

$$\frac{\Delta_j}{\omega_n} - \frac{|\Delta_j|^2 \Delta_j}{2\omega_n^3} - \frac{\hbar(\mathbf{v}_F^{(j)} \mathbf{\Pi}) \Delta_j}{2\omega_n^2} + \frac{\hbar^2(\mathbf{v}_F^{(j)} \mathbf{\Pi})(\mathbf{v}_F^{(j)} \mathbf{\Pi}) \Delta_j}{4\omega_n^3}$$

and $f_j^+(\mathbf{p}, \mathbf{r}, \omega_n) = f_j^*(-\mathbf{p}, \mathbf{r}, \omega_n)$. Then, for the summation over Matsubara frequencies, we get

$$2\pi T \sum_{n=0}^{N_d} \omega_n^{-1} = G_0 + \tau \quad (\text{A.5})$$

where $\tau = (1 - T/T_c)$. We normalize gaps by $T_c/\sqrt{\rho}$, where

$$\rho = \sum_{n=0}^{\infty} \frac{\pi T_c^3}{\omega_n^3} = \frac{7\zeta(3)}{8\pi^2} \approx 0.1, \quad (\text{A.6})$$

substitute (A.4) into the self-consistency Eqs.(A.2) and get the system of GL equations

$$[(G_0 + \tau - \hat{\Lambda}^{-1}) \mathbf{\Delta}]_j = -K_{ab}^{(j)} \Pi_a \Pi_b \Delta_j + |\Delta_j|^2 \Delta_j, \quad (\text{A.7})$$

Here $\mathbf{\Delta} = (\Delta_1, \Delta_2, \Delta_3)^T$, and the anisotropy tensor is $K_{ab}^{(j)} = \hbar^2 \rho \langle v_{Fa}^{(j)} v_{Fb}^{(j)} \rangle / 2T_c^2$ where the average is taken over the j -th Fermi surface and a, b stand for the x, y coordinates. The current is given by

$$\mathbf{j}(\mathbf{r}) = \frac{4e\nu T_c^2}{\hbar \rho} \sum_i \text{Im } \Delta_i^* \hat{K}_i \mathbf{\Pi} \Delta_i. \quad (\text{A.8})$$

In the following, we consider coupling matrix $\hat{g} = \nu_0 \hat{\Lambda}$ describing the case of an interband dominated pairing with repulsion. We assume that the density of states is

the same in all bands $\nu_{1,2,3} = \nu_0$ and parametrize different pairing interactions with two dimensionless coefficients η and ν as follows

$$\hat{\Lambda} = - \begin{pmatrix} 0 & \eta & \lambda \\ \eta & 0 & \lambda \\ \lambda & \lambda & 0 \end{pmatrix}. \quad (\text{A.9})$$

Here the coefficients describe different pairing channels in $s_{\pm} + is$ and $s + id$ states. In the former case $\Delta_{1,2}$ correspond to the gaps at hole Fermi surfaces and Δ_3 is the gap at electron pockets so that $u_{hh} = \nu_0\eta$ and $u_{eh} = \nu_0\lambda$ are the hole-hole and electron-hole interactions correspondingly. In contrast to describe the $s + id$ state we use the same model (A.9) but assume that $\Delta_{1,2}$ describe gaps in electron pockets and Δ_3 is the gap at the hole Fermi surface so that $u_{eh} = \nu_0\eta$ and $u_{ee} = \nu_0\lambda$ to be electron-hole and electron-electron interactions correspondingly.

Neglecting the r.h.s. in (A.7) we get the linear equation which determines the critical temperature $G_0 = \min(G_1, G_2)$, where $G_1 = 1/\eta$ and $G_2 = (\eta + \sqrt{\eta^2 + 8\lambda^2})/4\lambda^2$ are the positive eigenvalues of the matrix

$$\hat{\Lambda}^{-1} = \frac{1}{2\lambda^2\eta} \begin{pmatrix} \lambda^2 & -\lambda^2 & -\lambda\eta \\ -\lambda^2 & \lambda^2 & -\lambda\eta \\ -\lambda\eta & -\lambda\eta & \eta^2 \end{pmatrix}. \quad (\text{A.10})$$

The coupling matrix $\hat{\Lambda}^{-1}$ has only two positive eigenvalues $G_{1,2}$ whose eigenvectors are $\Delta_1 = (-1, 1, 0)^T$ and $\Delta_2 = (x, x, 1)^T$ with $x = (\eta - \sqrt{\eta^2 + 8\lambda^2})/4\lambda$. Since only the fields corresponding to the positive eigenvalues can nucleate, the GL theory (A.7) has to be reduced to a two-component one. To implement this reduction we represent the general order parameter in terms of the superposition

$$\Delta = \psi_1 \Delta_1 + \psi_2 \Delta_2, \quad (\text{A.11})$$

so that

$$(\Delta_1, \Delta_2, \Delta_3) = (x\psi_2 - \psi_1, x\psi_2 + \psi_1, \psi_2). \quad (\text{A.12})$$

where $\psi_{1,2}$ are the complex order parameter fields that have different interpretation depending on the system considered. In the $s + is$ case ψ_1 and ψ_2 are the order parameter of s_{\pm} pairing channels between two concentric hole surfaces and between hole and electron surfaces correspondingly. For the system with $s + id$ symmetry, ψ_1 is the order parameter of the d wave channel in electron pockets and ψ_2 is the order parameter of s_{\pm} pairing between electron and hole surfaces.

Now, substituting the ansatz (A.11) into the system of Ginzburg-Landau equations (A.7) we obtain, after projection on the vectors $\Delta_{1,2}$, the system of two GL equations

tions

$$a_1\psi_1 + b_{1j}|\psi_j|^2\psi_1 + b_J\psi_1^*\psi_2^2 = \quad (\text{A.13a})$$

$$(K_{aa}^{(1)} + K_{aa}^{(2)})\Pi_a^2\psi_1 + x(K_{aa}^{(2)} - K_{aa}^{(1)})\Pi_a^2\psi_2$$

$$a_2\psi_2 + b_{2j}|\psi_j|^2\psi_2 + b_J\psi_2^*\psi_1^2 = \quad (\text{A.13b})$$

$$\left[x^2(K_{aa}^{(1)} + K_{aa}^{(2)}) + K_{aa}^{(3)} \right] \Pi_a^2\psi_2 + x(K_{aa}^{(2)} - K_{aa}^{(1)})\Pi_a^2\psi_1.$$

The parameters of the left hand side of the Ginzburg-Landau equations (A.13) are expressed, in terms of the coefficients of the coupling matrix (A.9) as

$$a_j = -|\Delta_j|^2(G_0 - G_j + \tau), \quad (\text{A.14a})$$

$$\text{with } |\Delta_1|^2 = 2 \text{ and } |\Delta_2|^2 = 2x^2 + 1 \quad (\text{A.14b})$$

$$b_{11} = 2, \quad b_{22} = (2x^4 + 1) \text{ and } b_k := b_{kk} \quad (\text{A.14c})$$

$$b_{12} = 4x^2, \quad b_J = 2x^2. \quad (\text{A.14d})$$

The system (A.13) is quite general and describes both $s + is$ and $s + id$ states. The difference between these two cases is determined by the symmetry of gradient terms. In $s + is$ state the C_4 symmetry requires that $K_{xx}^{(j)} = K_{yy}^{(j)} = K^{(j)}$. Then the general Eqs. (A.13) are simplified as follows

$$\begin{aligned} a_1\psi_1 + b_{1j}|\psi_j|^2\psi_1 + b_J\psi_1^*\psi_2^2 &= k_{1j}\Pi^2\psi_j \\ a_2\psi_2 + b_{2j}|\psi_j|^2\psi_2 + b_J\psi_2^*\psi_1^2 &= k_{2j}\Pi^2\psi_j \end{aligned} \quad (\text{A.15})$$

where

$$\begin{aligned} k_{11} &= K^{(1)} + K^{(2)} \\ k_{22} &= [(K^{(1)} + K^{(2)})x^2 + K^{(3)}] \\ k_{12} &= x[K^{(2)} - K^{(1)}]. \end{aligned} \quad (\text{A.16})$$

In $s + id$ state the C_4 symmetry is broken so that $K_{xx}^{(1,2)} = K_{yy}^{(2,1)} = K^{(1,2)}$, where the bands 1, 2 correspond to the electron pockets. The hole band 3 is considered to be C_4 symmetric so that $K_{xx}^{(3)} = K_{yy}^{(3)} = K^{(3)}$. Then we obtain from Eqs.(A.13)

$$a_1\psi_1 + b_{1j}|\psi_j|^2\psi_1 + b_J\psi_1^*\psi_2^2 = \quad (\text{A.17a})$$

$$k_{11}\Pi^2\psi_1 + k_{12}\Pi_{xy}\psi_2$$

$$a_2\psi_2 + b_{2j}|\psi_j|^2\psi_2 + b_J\psi_2^*\psi_1^2 = \quad (\text{A.17b})$$

$$k_{22}\Pi^2\psi_2 + k_{12}\Pi_{xy}\psi_1$$

where the coefficients k_{ab} are given by the same Eq. (A.16) as in $s + is$ state and $\Pi_{xy} = \Pi_x^2 - \Pi_y^2$.

The general free energy functional which gives both the GL equations (A.15, A.17) is thus given by $F = \frac{B^2}{8\pi} + B_0^2 \tilde{F}_s$ where

$$\begin{aligned} \tilde{F}_s &= \sum_{j=1}^2 \left\{ k_{jj} |\Pi\psi_j|^2 + \alpha_j |\psi_j|^2 + \frac{\beta_j}{2} |\psi_j|^4 \right\} \\ &+ k_{12,a} \left((\Pi_a\psi_1)^* \Pi_a\psi_2 + c.c. \right) + \gamma |\psi_1|^2 |\psi_2|^2 \\ &+ \frac{\delta}{2} (\psi_1^{*2} \psi_2^2 + c.c.). \end{aligned} \quad (\text{A.18})$$

We denote $B_0 = T_c \sqrt{\nu_0/\rho}$ which is of the order the thermodynamical critical field at low temperatures [53]. An extra factor of ρ here comes from our normalization of gaps.

In the case of $s + is$ symmetry, $k_{12,x} = k_{12,y} \equiv k_{12}$, while for $s + id$ symmetry the mixed gradients satisfy $k_{12,x} = -k_{12,y} \equiv k_{12}$. The other coefficients are given by $\alpha_k = a_k$, $\beta_k = b_{kk}$, $\gamma = b_{12}$ and $\delta = b_J$.

Appendix B: Time-dependent Ginzburg-Landau theory for multicomponent superconductors

The time-dependent GL theory formally applies only in the gapless regime when either the inelastic electron-phonon relaxation τ_{ph}^{-1} or spin flip τ_{sf}^{-1} rates are much larger than the superconducting pairing amplitude. We will consider here the former scenario which realizes in the vicinity of the critical temperature $T_c - T \ll \tau_{ph}^{-1}$. In this case, the time-dependence is added to the generic Eqs.(A.15,A.17) in quite a standard way, following the derivation for a single-component case [50]

$$\begin{aligned} [(G_0 + \tau - \hat{\Lambda}^{-1})\Delta]_j = \\ \frac{\hbar\pi}{8T_c} \left(\frac{\partial}{\partial t} + \frac{2ie}{\hbar}\varphi \right) \Delta_j - K_{ab}^{(j)} \Pi_a \Pi_b \Delta_j + |\Delta_j|^2 \Delta_j, \end{aligned} \quad (\text{B.1})$$

Implementing the same reduction as in the stationary case, we obtain the system of two coupled TDGL equations:

$$\Gamma_k \left(\frac{\partial}{\partial t} + \frac{2ie}{\hbar}\varphi \right) \psi_k = -\frac{\delta\mathcal{F}}{\delta\psi_k^*}, \quad \frac{4\pi}{c} \nabla \times \mathbf{B} - \sigma_n \mathbf{E} = \mathbf{j}_s \quad (\text{B.2})$$

where $k = 1, \dots, N$, $\Gamma_k = |\Delta_k|^2 \pi \hbar B_0^2 / (8T_c)$ are the damping constants, φ is the scalar potential of electric field, σ_n is the normal state conductivity. The electric field is $\mathbf{E} = -c^{-1} \partial_t \mathbf{A} - \nabla \varphi$ where φ is electrostatic potential and for the superfluid current we have an expression $\mathbf{j}_s = -c \delta \mathcal{F} / \delta \mathbf{A}$. In the following since $|\Delta_{1,2}|^2 \approx 1$ we put $\Gamma_{1,2} = \Gamma = \pi \hbar B_0^2 / (8T_c)$.

In order to perform numerical simulations we normalize lengths by $\xi_0 = \hbar v_F / T_c$, where v_F is the average value of Fermi velocity, magnetic field by $B_0 = T_c \sqrt{\nu_0/\rho}$, free energy density by $F_0 = B_0^2$, current density by $j_0 = c B_0 / \xi_0$, time by $t_0 = \Gamma / B_0^2$, electric field by $E_0 = \xi_0 B_0 / (t_0 c)$, conductivity by $\sigma_0 = c^2 \Gamma / (\xi_0^2 B_0^2)$. In such units the electron charge is replaced by an effective coupling constant $\tilde{e} = \pi B_0 \xi_0^2 / \Phi_0$ which parametrizes the regimes of extremely type-II and type-I superconductivity at $\tilde{e} \ll 1$ and $\tilde{e} \gg 1$ respectively. To estimate the characteristic relaxation time we note that $t_0 = \pi \hbar / 8 T_c \sim 1 \text{ ps}$ provided $T_c \sim 1 \text{ meV}$ which is about 10 K.

The normal state electric conductivity σ_n in (B.2) can be defined from the Drude model. Up to unimportant numerical coefficient resulting from the Fermi surface anisotropy, it yields $\sigma_n \sim e^2 \nu_0 \bar{v}_F^2 \tau$, where τ is

a transport time. This estimation does not depend on whether superconductor is in the clean or diffusive limit since σ_n is a normal state characteristic. The dimensionless conductivity in our units is given by $\sigma_n / \sigma_0 \sim (\bar{v}_F / c)^2 (\varepsilon_F / T_c) (\hbar \tau \varepsilon_F)$, where ε_F is the Fermi energy. Here the first factor is small since typically $(\bar{v}_F / c)^2 \sim 10^{-5}$ in metals. The last two factors are large since $(\varepsilon_F / T_c) \sim 10^2$ and hence $(\hbar \tau \varepsilon_F) \sim 10^2 (\hbar \tau T_c)$. In this case in order to fulfil the clean limit conditions $(\tau T_c) > 1$ we need to assume the values of dimensionless conductivity $\sigma_n / \sigma_0 > 0.1$.

In dimensionless units the TDGL equations read

$$\left(\frac{\partial}{\partial t} + 2\tilde{e}\varphi \right) \psi_k = -\frac{\delta\mathcal{F}}{\delta\psi_k^*}, \quad \nabla \times \mathbf{B} - \sigma_n \mathbf{E} = \mathbf{j}_s \quad (\text{B.3})$$

where $\mathbf{E} = -\partial_t \mathbf{A} - \nabla \varphi$ and $\mathbf{j}_s = -\delta \mathcal{F} / \delta \mathbf{A}$. The free energy is given by

$$\begin{aligned} \mathcal{F} = \frac{B^2}{8\pi} + \sum_{j=1}^2 \left\{ k_{jj} |\Pi \psi_j|^2 + \alpha_j |\psi_j|^2 + \frac{\beta_j}{2} |\psi_j|^4 \right\} \\ + k_{12,a} \left((\Pi_a \psi_1)^* \Pi_a \psi_2 + c.c. \right) + \gamma |\psi_1|^2 |\psi_2|^2 \\ + \frac{\delta}{2} (\psi_1^{*2} \psi_2^2 + c.c.). \end{aligned} \quad (\text{B.4})$$

where $\Pi = \nabla - 2i\tilde{e}\mathbf{A}$.

Appendix C: Numerical methods and starting guess

We consider here the problem (B.2) defined on a two-dimensional bounded domain $\Omega \subset \mathbb{R}^2$ with $\partial\Omega$ its boundary. This problem is supplemented by the insulator boundary conditions, that no supercurrent flows through the boundary. The absence of supercurrent flowing through the boundary reads as $\mathbf{n} \cdot \Pi \psi_a = 0$ with \mathbf{n} the normal vector to $\partial\Omega$. The problem are then discretized using a finite element formulation provided by the **Freefem++** library [54]. Discretization of the integration domain Ω is done using a (homogeneous) triangulation over Ω , based on Delaunay-Voronoi algorithm. The fields are decomposed on a continuous piecewise quadratic basis on each triangle.

Numerical procedure

In our simulations, we chose the relaxation factor for the components of the order parameter $\Gamma = 1$ and the normal state conductivity $\sigma_n = 0.1$. We chose the gauge coupling constant $\tilde{e} = 0.2$ and the coefficients of the coupling matrix (A.9), that determine the coefficients of the Ginzburg-Landau functional (B.4), are $\eta = 5$ and $\lambda = 4.5$. The coefficients in GL functional (B.4) are then consistently obtained using the previously defined relations and the obtained values are $\beta_1 = 2$, $\beta_2 = 1.1079$,

$\delta = 0.4645$ and $\gamma = 0.929$. Given the coefficients of gradient terms in different bands are $K^{(1)} = 0.5$, $K^{(2)} = 0.05$, $K^{(3)} = 0.25$ and using the relation (A.17), the coefficients of the kinetic terms read as $k_1 = 0.55$, $k_2 = 0.375$ and $k_{12,x} = 0.217$, while $k_{12,y} = k_{12,x}$ for $s + is$ states and $k_{12,y} = -k_{12,x}$ for $s + id$. We are interested here in the effect of inhomogeneities of the order parameter induced by a local heating. In first approximation, temperature dependence within the Ginzburg-Landau theory is modelled by a linear dependence of the quadratic couplings on temperature: $\alpha_k(T) = a_k - \tau$, where $\tau = (1 - T/T_c)$ is the reduced temperature and a_k , a positive characteristic constants determined from the microscopic calculations, see Appendix A). As the Ginzburg-Landau expansion can be justified only in the vicinity of T_c , only a small interval of τ can be investigated.

The spatial modulation of the temperature is modelled as follow. Let Γ_0 denote the outer boundary of the domain (the sample's boundary) and Γ_1 an inner boundary (the heat source). In our simulations we considered various shapes of Γ_1 , but the results reported here are for Γ_1 to be a small circle. The temperature profile $T(\mathbf{x})$ is determined by solving the stationary heat equation with a small damping factor μ

$$\Delta T(\mathbf{x}) = \mu T(\mathbf{x}) \quad \text{and} \quad T(\Gamma_i) = \text{cte}. \quad (\text{C.1})$$

In our simulations, we set $T(\Gamma_0) = T_0 = 0.7T_c$ for the sample's boundary. On the other hand, the temperature of the source T_s varies with time as:

$$T_s(t) = T_0 + \frac{T_1 - T_0}{2} \left(1 - \cos \left(2\pi \frac{[t]}{n_T \Delta t} \right) \right) \quad (\text{C.2})$$

where $[x]$ denotes the floor function, $T_1 = 0.95T_c$ is the maximal temperature of the source and n_T is the number of heat source temperatures. In our simulations, we chose $n_T = 30$. Fig. 5 shows a typical solution for the stationary heat equation (C.1). Note that our choice here for considering the temperature profile given by the stationary heat equation implies that we assume that heat transport occurs on time scales much smaller than the other time scales of the problem.

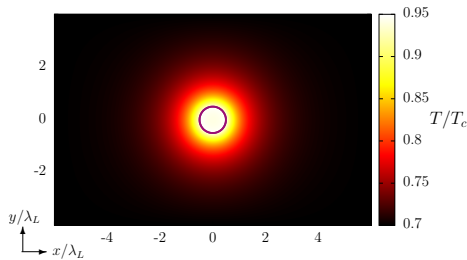


Figure 5: (Color online) – Temperature profile obtained by solving the stationary heat equation (C.1) for a local heating of the sample. The inhomogeneous temperature profile is induced by the ring-like heat source shown by the (purple) circle.

The heat equation (C.1) is thus solved for a given temperature T_s of the heat source (Γ_1). This defines the temperature profile $T(\mathbf{x}, t)$ and thus the spatial modulation quadratic couplings $\alpha_i(T) = a_i - \tau$. The time dependent Ginzburg-Landau equations (B.2) are discretized using Euler's forward method and iterated for a given interval $\Delta t = N\delta t$. The time step δt depends on the various time scales of the problem. Here we chose $\delta t = 10^{-2}$ and $N = 8 \times 10^3$. After Δt , the procedure is repeated for a new temperature T_s of the heat source given by (C.2).

Starting guess for domain-walls

The starting solutions are stationary solutions of the GL functional, for constant temperature. That is with no heat source. They can simply be ground state but also topologically non-trivial solutions in equilibrium. Domain-walls are topological excitations that are associated with the spontaneous breakdown of a discrete symmetry. These are field configurations that interpolate between inequivalent ground-states that are disconnected. Here, we are in particular interested in domain-walls that interpolate between regions with inequivalent relative phases between the condensates. When the ground-state breaks time-reversal symmetry, its complex conjugate is not a gauge equivalent. That is, there exist no real number χ_0 such that $\Psi_0^* = e^{i\chi_0} \Psi_0$. If no such transformation exists, then $\Psi_0^* \not\equiv \Psi_0$ and the configurations with ground state phases $\bar{\varphi}_a$ and $-\bar{\varphi}_a$ are disconnected and degenerate in energy. Domain-walls that interpolate between Ψ_0 and Ψ_0^* are topologically protected as their unwinding would require to overcome an infinite energy barrier, see for example textbook discussion in [65, 66]. The domain-wall that interpolates between Ψ_0^* and Ψ_0 can thus be parametrized by:

$$\psi_a^{(dw)} = u_a \exp \left[i \bar{\varphi}_a \tanh \left(\frac{\mathbf{x}_\perp - \mathbf{x}_0}{\xi_a^{(dw)}} \right) \right] \quad (\text{C.3})$$

where \mathbf{x}_0 is the curvilinear abscissa that gives the position of the domain-wall, and \mathbf{x}_\perp is the coordinate perpendicular to the domain-wall and $\xi_a^{(dw)}$ determines the width of the domain-wall.

Appendix D: Description Additional Movie Material

- Movie **Anim-magnetic.avi**:
shows the evolution of the magnetic response that originates in time-varying local heating of the sample. Detailed description is given in the caption of Fig. 6.
- Movie **Anim-imbalance.avi**:
shows the evolution of the electric response that originates in non-stationary local of the sample. Detailed description is given in the caption of Fig. 7.

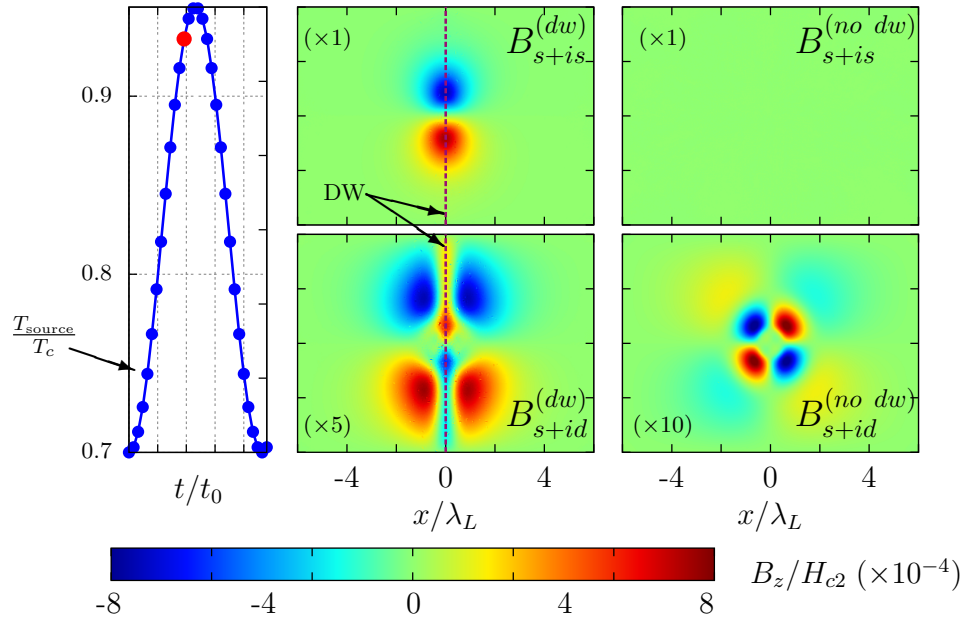


Figure 6: (Color online) – Evolution of the magnetic response that originates in time-varying local heating of the sample. The overall time sequence runs for $t/t_0 = 2400$. The leftmost panel shows the time evolution of the source’s temperature given by (C.2) and the red dot denotes the position in the time series. This corresponds to Figure 2 of the main text. The color plot shows the magnitude of the out-of-plane induced magnetic field B_z in unit of the second critical field. The two upper panels show the response of an $s + is$ superconducting state respectively with a domain wall and the homogeneous state. The two lower panels show the response of an $s + id$ superconducting state respectively with a domain wall and the homogeneous (anisotropic) state.

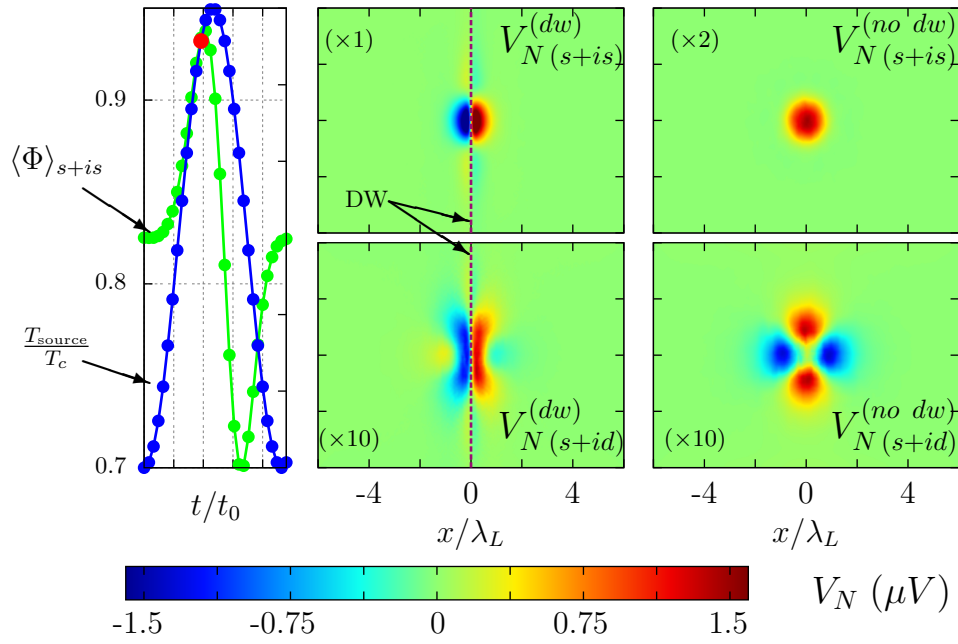


Figure 7: (Color online) – Evolution of the electric response that originates in time-varying local heating of the sample. The overall time sequence runs for $t/t_0 = 2400$. The leftmost panel shows the time evolution of the source’s temperature given by (C.2) and the red dot denotes the position in the time series. This corresponds to Figure 3 of the main text. The color plot shows the voltage induced in the normal detector by the charge imbalance due to the non-stationary heating. The two upper panels show the response of an $s + is$ superconducting state respectively with a domain wall and the homogeneous state. The two lower panels show the response of an $s + id$ superconducting state respectively with a domain wall and the homogeneous (anisotropic) state.

-
- [1] I.I. Mazin and V.P. Antropov, “Electronic structure, electron–phonon coupling, and multiband effects in MgB_2 ,” *Physica C: Superconductivity* **385**, 49 – 65 (2003).
- [2] A. Damascelli, D. H. Lu, K. M. Shen, N. P. Armitage, F. Ronning, D. L. Feng, C. Kim, Z.-X. Shen, T. Kimura, Y. Tokura, Z. Q. Mao, and Y. Maeno, “Fermi Surface, Surface States, and Surface Reconstruction in Sr_2RuO_4 ,” *Phys. Rev. Lett.* **85**, 5194–5197 (2000).
- [3] Yoichi Kamihara, Takumi Watanabe, Masahiro Hirano, and Hideo Hosono, “Iron-Based Layered Superconductor $\text{La}[\text{O}_{1-x}\text{F}_x]\text{FeAs}$ ($x = 0.05\text{--}0.12$) with $T_c = 26\text{ K}$,” *Journal of the American Chemical Society* **130**, 3296–3297 (2008).
- [4] I. I. Mazin, D. J. Singh, M. D. Johannes, and M. H. Du, “Unconventional Superconductivity with a Sign Reversal in the Order Parameter of $\text{LaFeAsO}_{1-x}\text{F}_x$,” *Phys. Rev. Lett.* **101**, 057003 (2008).
- [5] Kazuhiko Kuroki, Seiichiro Onari, Ryotaro Arita, Hidetomo Usui, Yukio Tanaka, Hiroshi Kontani, and Hideo Aoki, “Unconventional Pairing Originating from the Disconnected Fermi Surfaces of Superconducting $\text{LaFeAsO}_{1-x}\text{F}_x$,” *Phys. Rev. Lett.* **101**, 087004 (2008).
- [6] A. V. Chubukov, D. V. Efremov, and I. Eremin, “Magnetism, superconductivity, and pairing symmetry in iron-based superconductors,” *Phys. Rev. B* **78**, 134512 (2008).
- [7] A.V. Balatsky, “Field-induced $d_{x^2-y^2} + id_{xy}$ state and marginal stability of high- T_c superconductor,” *Physica C: Superconductivity* **332**, 337 – 342 (2000).
- [8] Wei-Cheng Lee, Shou-Cheng Zhang, and Congjun Wu, “Pairing State with a Time-Reversal Symmetry Breaking in FeAs-Based Superconductors,” *Phys. Rev. Lett.* **102**, 217002 (2009).
- [9] Christian Platt, Ronny Thomale, Carsten Honerkamp, Shou-Cheng Zhang, and Werner Hanke, “Mechanism for a pairing state with time-reversal symmetry breaking in iron-based superconductors,” *Phys. Rev. B* **85**, 180502 (2012).
- [10] Valentin Stanev and Zlatko Tešanović, “Three-band superconductivity and the order parameter that breaks time-reversal symmetry,” *Phys. Rev. B* **81**, 134522 (2010).
- [11] Rafael M. Fernandes and Andrew J. Millis, “Nematicity as a Probe of Superconducting Pairing in Iron-Based Superconductors,” *Phys. Rev. Lett.* **111**, 127001 (2013).
- [12] D. F. Agterberg, Victor Barzykin, and Lev P. Gor’kov, “Conventional mechanisms for exotic superconductivity,” *Phys. Rev. B* **60**, 14868–14871 (1999).
- [13] T. K. Ng and N. Nagaosa, “Broken time-reversal symmetry in Josephson junction involving two-band superconductors,” *Europhysics Letters* **87**, 17003–+ (2009).
- [14] Shi-Zeng Lin and Xiao Hu, “Massless Leggett Mode in Three-Band Superconductors with Time-Reversal-Symmetry Breaking,” *Phys. Rev. Lett.* **108**, 177005 (2012).
- [15] Johan Carlström, Julien Garaud, and Egor Babaev, “Length scales, collective modes, and type-1.5 regimes in three-band superconductors,” *Phys. Rev. B* **84**, 134518 (2011).
- [16] A. M. Bobkov and I. V. Bobkova, “Time-reversal symmetry breaking state near the surface of an s_{\pm} superconductor,” *Phys. Rev. B* **84**, 134527 (2011).
- [17] Saurabh Maiti and Andrey V. Chubukov, “ $s + is$ state with broken time-reversal symmetry in Fe-based superconductors,” *Phys. Rev. B* **87**, 144511 (2013).
- [18] Saurabh Maiti, Manfred Sigrist, and Andrey Chubukov, “Spontaneous currents in a superconductor with $s + is$ symmetry,” *Phys. Rev. B* **91**, 161102 (2015).
- [19] A. D. Christianson, E. A. Goremychkin, R. Osborn, S. Rosenkranz, M. D. Lumsden, C. D. Malliakas, I. S. Todorov, H. Claus, D. Y. Chung, M. G. Kanatzidis, R. I. Bewley, and T. Guidi, “Unconventional superconductivity in $\text{Ba}_{0.6}\text{K}_{0.4}\text{Fe}_2\text{As}_2$ from inelastic neutron scattering,” *Nature* **456**, 930–932 (2008).
- [20] X. G. Luo, M. A. Tanatar, J.-Ph. Reid, H. Shakeripour, N. Doiron-Leyraud, N. Ni, S. L. Bud’ko, P. C. Canfield, Huiqian Luo, Zhaosheng Wang, Hai-Hu Wen, R. Prozorov, and Louis Taillefer, “Quasiparticle heat transport in single-crystalline $\text{Ba}_{1-x}\text{K}_x\text{Fe}_2\text{As}_2$: Evidence for a k -dependent superconducting gap without nodes,” *Phys. Rev. B* **80**, 140503 (2009).
- [21] H. Ding, P. Richard, K. Nakayama, K. Sugawara, T. Arakane, Y. Sekiba, A. Takayama, S. Souma, T. Sato, T. Takahashi, Z. Wang, X. Dai, Z. Fang, G. F. Chen, J. L. Luo, and N. L. Wang, “Observation of Fermi-surface-dependent nodeless superconducting gaps in $\text{Ba}_{0.6}\text{K}_{0.4}\text{Fe}_2\text{As}_2$,” *EPL (Europhysics Letters)* **83**, 47001 (2008).
- [22] R. Khasanov, D. V. Evtushinsky, A. Amato, H.-H. Klauss, H. Luetkens, Ch. Niedermayer, B. Büchner, G. L. Sun, C. T. Lin, J. T. Park, D. S. Inosov, and V. Hinkov, “Two-Gap Superconductivity in $\text{Ba}_{1-x}\text{K}_x\text{Fe}_2\text{As}_2$: A Complementary Study of the Magnetic Penetration Depth by Muon-Spin Rotation and Angle-Resolved Photoemission,” *Phys. Rev. Lett.* **102**, 187005 (2009).
- [23] K. Nakayama, T. Sato, P. Richard, Y.-M. Xu, T. Kawahara, K. Umezawa, T. Qian, M. Neupane, G. F. Chen, H. Ding, and T. Takahashi, “Universality of superconducting gaps in overdoped $\text{Ba}_{0.3}\text{K}_{0.7}\text{Fe}_2\text{As}_2$ observed by angle-resolved photoemission spectroscopy,” *Phys. Rev. B* **83**, 020501 (2011).
- [24] S. Maiti, M. M. Korshunov, T. A. Maier, P. J. Hirschfeld, and A. V. Chubukov, “Evolution of the Superconducting State of Fe-Based Compounds with Doping,” *Phys. Rev. Lett.* **107**, 147002 (2011).
- [25] S. Maiti, M. M. Korshunov, T. A. Maier, P. J. Hirschfeld, and A. V. Chubukov, “Evolution of symmetry and structure of the gap in iron-based superconductors with doping and interactions,” *Phys. Rev. B* **84**, 224505 (2011).
- [26] J-Ph Reid, A Juneau-Fecteau, R T Gordon, S René de Cotret, N Doiron-Leyraud, X G Luo, H Shakeripour, J Chang, M A Tanatar, H Kim, R Prozorov, T Saito, H Fukazawa, Y Kohori, K Kihou, C H Lee, A Iyo, H Eisaki, B Shen, H-H Wen, and Louis Taillefer, “From d-wave to s-wave pairing in the iron-pnictide superconductor $(\text{Ba},\text{K})\text{Fe}_2\text{As}_2$,” *Superconductor Science and Technology* **25**, 084013 (2012).
- [27] J.-Ph. Reid, M. A. Tanatar, A. Juneau-Fecteau, R. T. Gordon, S. R. de Cotret, N. Doiron-Leyraud, T. Saito, H. Fukazawa, Y. Kohori, K. Kihou, C. H. Lee, A. Iyo, H. Eisaki, R. Prozorov, and Louis Taillefer, “Universal Heat Conduction in the Iron Arsenide Superconductor

- KFe₂As₂: Evidence of a d -Wave State,” *Phys. Rev. Lett.* **109**, 087001 (2012).
- [28] F. F. Tafti, A. Juneau-Fecteau, M-E. Delage, S. Rene de Cotret, J-Ph. Reid, A. F. Wang, X-G. Luo, X. H. Chen, N. Doiron-Leyraud, and Louis Taillefer, “Sudden reversal in the pressure dependence of T_c in the iron-based superconductor KFe₂As₂,” *Nature Physics* **9**, 349–352 (2013).
- [29] F. F. Tafti, J. P. Clancy, M. Lapointe-Major, C. Collignon, S. Faucher, J. A. Sears, A. Juneau-Fecteau, N. Doiron-Leyraud, A. F. Wang, X.-G. Luo, X. H. Chen, S. Desgreniers, Young-June Kim, and Louis Taillefer, “Sudden reversal in the pressure dependence of T_c in the iron-based superconductor CsFe₂As₂: A possible link between inelastic scattering and pairing symmetry,” *Phys. Rev. B* **89**, 134502 (2014).
- [30] D. Watanabe, T. Yamashita, Y. Kawamoto, S. Kurata, Y. Mizukami, T. Ohta, S. Kasahara, M. Yamashita, T. Saito, H. Fukazawa, Y. Kohori, S. Ishida, K. Kihou, C. H. Lee, A. Iyo, H. Eisaki, A. B. Vorontsov, T. Shibauchi, and Y. Matsuda, “Doping evolution of the quasiparticle excitations in heavily hole-doped Ba_{1-x}K_xFe₂As₂: A possible superconducting gap with sign-reversal between hole pockets,” *Phys. Rev. B* **89**, 115112 (2014).
- [31] K. Okazaki, Y. Ota, Y. Kotani, W. Malaeb, Y. Ishida, T. Shimojima, T. Kiss, S. Watanabe, C.-T. Chen, K. Kihou, C. H. Lee, A. Iyo, H. Eisaki, T. Saito, H. Fukazawa, Y. Kohori, K. Hashimoto, T. Shibauchi, Y. Matsuda, H. Ikeda, H. Miyahara, R. Arita, A. Chainani, and S. Shin, “Octet-Line Node Structure of Superconducting Order Parameter in KFe₂As₂,” *Science* **337**, 1314–1317 (2012).
- [32] Robert Joynt, “Upward curvature of H_{c2} in high- T_c superconductors: Possible evidence for s - d pairing,” *Phys. Rev. B* **41**, 4271–4277 (1990).
- [33] Q. P. Li, B. E. C. Koltenbah, and Robert Joynt, “Mixed s -wave and d -wave superconductivity in high- T_c systems,” *Phys. Rev. B* **48**, 437–455 (1993).
- [34] A. J. Berlinsky, A. L. Fetter, M. Franz, C. Kallin, and P. I. Soininen, “Ginzburg-Landau Theory of Vortices in d -Wave Superconductors,” *Phys. Rev. Lett.* **75**, 2200–2203 (1995).
- [35] V.R. Misko, V.M. Fomin, J.T. Devreese, and V.V. Moshchalkov, “On the Ginzburg-Landau analysis of a mixed s - $d_{x^2-y^2}$ -wave superconducting mesoscopic square,” *Solid State Communications* **114**, 499 – 504 (2000).
- [36] M. Franz and Z. Tešanović, “Self-Consistent Electronic Structure of a $d_{x^2-y^2}$ and a $d_{x^2-y^2} + id_{xy}$ Vortex,” *Phys. Rev. Lett.* **80**, 4763–4766 (1998).
- [37] Andrew Peter Mackenzie and Yoshiteru Maeno, “The superconductivity of Sr₂RuO₄ and the physics of spin-triplet pairing,” *Rev. Mod. Phys.* **75**, 657–712 (2003).
- [38] Valentin Stanev, “Model of collective modes in three-band superconductors with repulsive interband interactions,” *Phys. Rev. B* **85**, 174520 (2012).
- [39] M. Marciani, L. Fanfarillo, C. Castellani, and L. Benfatto, “Leggett modes in iron-based superconductors as a probe of time-reversal symmetry breaking,” *Phys. Rev. B* **88**, 214508 (2013).
- [40] Julien Garaud, Johan Carlström, and Egor Babaev, “Topological Solitons in Three-Band Superconductors with Broken Time Reversal Symmetry,” *Phys. Rev. Lett.* **107**, 197001 (2011).
- [41] Julien Garaud, Johan Carlström, Egor Babaev, and Martin Speight, “Chiral CP^2 skyrmions in three-band superconductors,” *Phys. Rev. B* **87**, 014507 (2013).
- [42] Julien Garaud and Egor Babaev, “Domain Walls and Their Experimental Signatures in $s + is$ Superconductors,” *Phys. Rev. Lett.* **112**, 017003 (2014).
- [43] Mihail Silaev and Egor Babaev, “Unusual mechanism of vortex viscosity generated by mixed normal modes in superconductors with broken time reversal symmetry,” *Phys. Rev. B* **88**, 220504 (2013).
- [44] Troels Arnfred Bojesen, Egor Babaev, and Asle Sudbø, “Time reversal symmetry breakdown in normal and superconducting states in frustrated three-band systems,” *Phys. Rev. B* **88**, 220511 (2013).
- [45] Troels Arnfred Bojesen, Egor Babaev, and Asle Sudbø, “Phase transitions and anomalous normal state in superconductors with broken time-reversal symmetry,” *Phys. Rev. B* **89**, 104509 (2014).
- [46] Johan Carlström and Egor Babaev, “Spontaneous breakdown of time-reversal symmetry induced by thermal fluctuations,” *Phys. Rev. B* **91**, 140504 (2015).
- [47] Alberto Hinojosa, Rafael M. Fernandes, and Andrey V. Chubukov, “Time-Reversal Symmetry Breaking Superconductivity in the Coexistence Phase with Magnetism in Fe Pnictides,” *Phys. Rev. Lett.* **113**, 167001 (2014).
- [48] Mihail Silaev, Julien Garaud, and Egor Babaev, “Unconventional thermoelectric effect in superconductors that break time-reversal symmetry,” *Phys. Rev. B* **92**, 174510 (2015).
- [49] Ariel Maniv, Emil Polturak, Gad Koren, Yuri Bliokh, Björn Biehler, Bernd-Uwe Runge, Paul Leiderer, Boris Shapiro, and Irena Shapiro, “Observation of a New Mechanism of Spontaneous Generation of Magnetic Flux in a Superconductor,” *Phys. Rev. Lett.* **94**, 247005 (2005).
- [50] N. Kopnin, *Theory of Nonequilibrium Superconductivity*, International Series of Monographs on Physics (Oxford University Press, 2009).
- [51] Alan T. Dorsey, “Vortex motion and the Hall effect in type-II superconductors: A time-dependent Ginzburg-Landau theory approach,” *Phys. Rev. B* **46**, 8376–8392 (1992).
- [52] The lengths are normalized by $\tilde{\xi}_0 = \hbar \bar{v}_F / T_c$, where \bar{v}_F is the average value of Fermi velocity, magnetic field by $B_0 = T_c \sqrt{\nu_0 / \rho}$, where T_c is in energy units and $\rho = 7\zeta(3)/(8\pi^2) \approx 0.1$. The magnetic field scale B_0 is of the order the thermodynamic critical field at low temperatures [53]. In such units the electron charge is replaced by an effective coupling constant $\tilde{e} = \pi B_0 \xi_0^2 / \Phi_0$.
- [53] D. Saint-James, E.J. Thomas, and G. Sarma, *Type II Superconductivity*, International series of monographs in natural philosophy (Pergamon, 1970).
- [54] F. Hecht, “New development in freefem++,” *J. Numer. Math.* **20**, 251–265 (2012).
- [55] The consistently obtained values are $\beta_1 = 2$, $\beta_2 = 1.108$, $\delta = 0.465$ and $\gamma = 0.929$. The coefficients of the kinetic terms are $k_1 = 0.55$, $k_2 = 0.375$ and $k_{12,x} = 0.217$, while $k_{12,y} = k_{12,x}$ for $s + is$ states and $k_{12,y} = -k_{12,x}$ for $s + id$. See detailed derivation in Appendix A and B.
- [56] G. R. Stewart, “Superconductivity in iron compounds,” *Rev. Mod. Phys.* **83**, 1589–1652 (2011).
- [57] P. J. Curran, S. J. Bending, W. M. Desoky, A. S. Gibbs,

- S. L. Lee, and A. P. Mackenzie, “Search for spontaneous edge currents and vortex imaging in Sr_2RuO_4 mesostructures,” *Phys. Rev. B* **89**, 144504 (2014).
- [58] T. J. Rieger, D. J. Scalapino, and J. E. Mercereau, “Charge Conservation and Chemical Potentials in Time-Dependent Ginzburg-Landau Theory,” *Phys. Rev. Lett.* **27**, 1787–1790 (1971).
- [59] M. Tinkham and John Clarke, “Theory of Pair-Quasiparticle Potential Difference in Nonequilibrium Superconductors,” *Phys. Rev. Lett.* **28**, 1366–1369 (1972).
- [60] A.M. Kadin, L.N. Smith, and W.J. Skocpol, “Charge imbalance waves and nonequilibrium dynamics near a superconducting phase-slip center,” *Journal of Low Temperature Physics* **38**, 497–534 (1980).
- [61] John Clarke, “Experimental Observation of Pair-Quasiparticle Potential Difference in Nonequilibrium Superconductors,” *Phys. Rev. Lett.* **28**, 1363–1366 (1972).
- [62] M. L. Yu and J. E. Mercereau, “Nonequilibrium quasiparticle current at superconducting boundaries,” *Phys. Rev. B* **12**, 4909–4916 (1975).
- [63] Animations of non-stationary processes can be found as ancillary files. Or see webpage with embedded videos at: <http://www.theophys.kth.se/~garaud/hotspot.html>.
- [64] A. B. Vorontsov, I. Vekhter, and M. Eschrig, “Surface Bound States and Spin Currents in Noncentrosymmetric Superconductors,” *Phys. Rev. Lett.* **101**, 127003 (2008).
- [65] N. S. Manton and P. Sutcliffe, *Topological solitons* (Cambridge University Press, 2004) cambridge, UK: Univ. Pr. (2004) 493 p.
- [66] R. Rajaraman, *Solitons and Instantons. An Introduction to Solitons and Instantons in Quantum Field Theory* (North-Holland Publishing Company, Amsterdam, 1982).
- [67] The lengths are normalized by $\tilde{\xi}_0 = \hbar\bar{v}_F/T_c$, where \bar{v}_F is the average value of Fermi velocity, magnetic field by $B_0 = T_c\sqrt{\nu_0/\rho}$, where T_c is in energy units and $\rho = 7\zeta(3)/(8\pi^2) \approx 0.1$. The magnetic field scale B_0 is of the order the thermodynamic critical field at low temperatures [53]. In such units the electron charge is replaced by an effective coupling constant $\tilde{e} = \pi B_0 \xi_0^2 / \Phi_0$.
- [68] The consistently obtained values are $\beta_1 = 2$, $\beta_2 = 1.108$, $\delta = 0.465$ and $\gamma = 0.929$. The coefficients of the kinetic terms are $k_1 = 0.55$, $k_2 = 0.375$ and $k_{12,x} = 0.217$, while $k_{12,y} = k_{12,x}$ for $s+is$ states and $k_{12,y} = -k_{12,x}$ for $s+id$. See detailed derivation in Appendix A and B.